Localization of individual lightning discharges via directional and temporal triangulation of sferic measurements at two distant sites

T. G. Wood and U. S. Inan

Space, Telecommunications, and Radioscience Laboratory, Stanford University, Stanford, California, USA

Received 7 July 2004; revised 27 August 2004; accepted 8 September 2004; published 6 November 2004.

[1] Lightning discharges generate electromagnetic pulses, known as sferics, that propagate through the waveguide formed by the Earth and the ionosphere. The energy in the VLF band can propagate over great distances (~10,000 km) with low loss (3 dB/Mm) and can therefore be detected far from the source lightning location. Using sferic measurements from VLF receivers at Palmer Station, Antarctica, and Vieques Island, Puerto Rico, the locations of lightning discharges from regions such as South America, North America, and Africa are triangulated. Both sferic arrival azimuth at the two receivers and the time of arrival difference between the receivers are used to find the best estimate of the lightning discharge location. Owing to the extremely wide separation of the two receivers, ambiguities sometimes result in pairing sferics detected at one site to their matching sferics detected at the other site. In these cases a best-best estimate scheme is used. Simulation results indicate that for the two receivers considered here the most accurate location performance is in South America with an expected median location error of ~75 km. The system has the worst performance due north of the Vieques Island site, with an expected median location error of ~2000 km. Triangulation results for South America are shown for the period 7–10 September 2001. Results for 8 September 2001 are compared to cloud-to-ground lightning flashes detected by the National Lightning Detection Network. For this day, 49% of flashes were detected with a median error of about 200 km. Results are also compared to lightning discharges detected by the Lightning Imaging Sensor (LIS) aboard the Tropical Rainfall Measuring Mission (TRMM) satellite. For a particular TRMM pass over South America, 20% of flashes detected by LIS were correctly located using the described technique, with a median error of 187 km. The event rate for a localized South American storm is also monitored and documented for the same 4-day period. *INDEX TERMS:* 0604 Electromagnetics: Antenna arrays; 0624 Electromagnetics: Guided waves; 3304 Meteorology and Atmospheric Dynamics: Atmospheric electricity; 3324 Meteorology and Atmospheric Dynamics: Lightning; *KEYWORDS:* lightning, location, sferics

Citation: Wood, T. G., and U. S. Inan (2004), Localization of individual lightning discharges via directional and temporal triangulation of sferic measurements at two distant sites, *J. Geophys. Res.*, *109*, D21109, doi:10.1029/2004JD005204.

1. Introduction

[2] Lightning flash rate is a frequently quoted parameter for quantifying thunderstorm activity. The global flash rate provides an indication of the number of thunderstorms occurring worldwide [*Williams et al.*, 2000] and the flash rate for individual storms provides insight into a wide variety of thunderstorm parameters. For example, flash rate is related to storm updraft [*Baker et al.*, 1995, 1999], storm dimensions such as cloud height [*Shackford*, 1960; *Williams*, 1985; *Cherna and Stansbury*, 1986] and overall storm size [*Grosh*, 1978; *Cherna and Stansbury*, 1986] as well as to mesocyclone evolution [*MacGorman et al.*, 1989]. The total amount of lightning activity present in a storm can also provide an estimate of the amount of convective rainfall in that storm [*Rutledge et al.*, 1992; *Williams et al.*, 1992; *Petersen and Rutledge*, 1998; *Tapia et al.*, 1998; *Alexander et al.*, 1999; *Kempf and Krider*, 2003]. Furthermore, the spectral properties of radio atmospherics (or sferics in short), the electromagnetic impulses generated by lightning, reveal information about other phenomena. For example, the presence of an extremely low frequency (ELF) tail is related to the occurrence of sprites [*Reising et al.*, 1999] and the ratio of the ELF to VLF (very low frequency) energy in sferics has been tied to lighting source orientation [*Wood and Inan*, 2002]. However, the precise relationship of lightning characteristics to these different parameters is expected to vary from region to region around the world as there are very few relationships that are globally constant [*Boccippio et al.*, 2000]. Thus monitoring of lightning activity on a global scale is needed in order to attain a complete understanding of these relationships.

0148-0227/04/2004JD005204$09.00

[3] Many techniques have been employed for the detection and location of lightning discharges. From space, the Lightning Imaging Sensor (LIS) [*Christian et al.*, 1999] aboard the TRMM satellite and its predecessor the Optical Transient Detector (OTD) [*Christian et al.*, 2003] detect "total" lightning including both cloud-to-ground (CG) and intra-cloud (IC) lightning discharges using optical measurements. The low Earth orbit (350 km altitude) of TRMM and its relatively low inclination of 35° allows LIS to observe a particular spot continuously for almost 90 seconds at a time with ~5 km resolution.

[4] On the ground, many different methods of radiolocation of lightning have been implemented. For example, a single radio receiver can be used to locate intense lightning discharges at long range, by using the wave impedance of the lightning waveform to estimate the range to the lightning strike and by using magnetic direction finding to measure the arrival azimuth of the lightning strike [*Burke and Jones*, 1995; *Huang et al.*, 1999; *Price and Asfur*, 2002], which together determine the location of the source lightning event. Lightning discharges measured in this manner must be intense because a large ELF energy component, also called an ELF slow-tail, is generally required for the range estimate [*Burke and Jones*, 1995]. The most common methods for the radiolocation of lightning involve the use of measurements at multiple sites. Some of these methods rely on magnetic direction finding (MDF) [*Horner*, 1954; *Hiscox et al.*, 1984] while other methods use arrival time difference (ATD) [*Lewis et al.*, 1960; *Lee*, 1986, 1990; *Fullerkrug and Constable*, 2000; *Dowden et al.*, 2002]. There have also been some experiments that use both MDF and ATD for location [*Hughes and Gallenberger*, 1974]. The techniques used vary in complexity and the number of measurement sites as well as in accuracy and spatial coverage. In North America, the National Lightning Detection Network (NLDN) uses a combined ATD/MDF technique to detect cloud to ground (CG) lightning events by matching received broadband (~400 Hz–400 kHz) waveforms to the signature waveform expected from the direct wave of a CG lightning stroke [*Cummins et al.*, 1998]. This technique eliminates many of the errors caused by reflections from the ground and ionosphere as well as polarization errors [*Krider et al.*, 1976], but requires very wide band measurements of hundreds of kHz to MHz components of the sferic spectra that are too weak to measure at large distances. NLDN typically excludes intra-cloud (IC) lightning discharges from detection based on the fact that the waveforms of IC sferics are distinctly different from the characteristic waveforms for CG flashes[*Krider et al.*, 1976].

[5] The very low frequency band is most commonly used for long range radiolocation of lightning due to the highly efficient propagation of VLF sferic energy in the Earth-ionosphere waveguide. The attenuation for VLF propagation in the waveguide is ~3 dB/Mm, allowing for the detection of lightning at long distances (upwards of 10,000 km) [*Davies*, 1965, p. 367]. The fact that the group velocity is close to the speed of light for low order modes at VLF frequencies and does not significantly vary with frequency (away from the cutoff regions) [*Budden*, 1961, p. 69] further simplifies the analysis and ATD estimations. For example, using the equation for group velocity as taken from Budden, where f_n is the mode cutoff frequency, it can be shown

$$V_{group} = c\left\{1 - \left(\frac{f_n}{f}\right)^2\right\}^{-\frac{1}{2}} \quad (1)$$

that for VLF propagation at 13 kHz, the difference in propagation time for daytime (60 km reflection height) verses nighttime (80 km reflection height) for a 10,000 km path is ~280 microseconds, which would cause a smaller error than a one degree error in azimuth at 5,000 km. However, some techniques, such as those that rely only on ATD measurements, do require more precise knowledge of the group velocity under various propagation conditions [*Dowden et al.*, 2002].

[6] The technique presented in this paper combines magnetic direction finding with time of arrival difference using two very widely spaced receivers (>9,000 km) to determine lightning locations via triangulation. One receiver is located at Palmer Station (64.77°S, 64.05°W) on Anvers Island off the Antarctic peninsula while the other is located on Vieques Island (18.12°N, 65.50°W) off the coast of Puerto Rico. Palmer Station is ideally located for this type of application since it is remotely located from populated areas and most lightning locations, thus providing, respectively, comparatively low ambient noise background and lower polarization error due to relatively long propagation distances from source lightning. On the other hand, the Vieques Island site is relatively close to populated regions and therefore 60 Hz "noise" sources, and is also at an undesirably close range to many active lightning regions. In addition, the data collected from Vieques were part of a separate experiment with a recording schedule from 0005–0950 UT and 1635–2350 UT with recordings made for one minute every fifteen minutes, thus limiting the time of available sferics. Furthermore the receiver site was, unfortunately, subject to power outages and the data were sometimes subject to corruption due to saturation by the NAU VLF transmitter located at a distance of only a few hundred kilometers. Nevertheless, the technique described herein is general and can be applied to any two site locations and in fact provides encouraging results despite the drawbacks of the Vieques site.

2. Triangulation Technique

[7] The first step in determining lightning locations via triangulation with two widely separated sites is to calculate the sferic arrival azimuths at each site. The VLF antennas used in this experiment consist of two orthogonal crossed magnetic loop antennas that measure the horizontal magnetic field component of incoming waves. This arrangement necessarily introduces a 180 degree ambiguity into the azimuth calculation since, in general, the polarity of the electric field would also be needed to unambiguously determine arrival azimuth for incoming waves.

[8] The sferic waveforms are detected and their arrival azimuths are computed using the magnetic direction finding technique described by *Wood and Inan* [2002]. For the cases reported in this paper, we have used the 9–13 kHz band

instead of the 5.5–9.5 kHz band used in the previous study. This change was made because the Omega navigation transmitters that were active during the times of the data used for the first study have since been decommissioned and the peak signal strength for sferics occurs around 10 kHz. The direction finding technique operates with the underlying assumption that the detected sferics are predominantly composed of Transverse Magnetic (TM) waveguide modes. In other words, the technique is applied with the implicit assumption that the arrival azimuth of a sferic can be accurately determined by measuring the horizontal magnetic field component of the incoming wave. Since the magnetic field components of TM waves are transverse to the direction of propagation in the waveguide, the arrival azimuth is along the direction perpendicular to the magnetic field vector in the plane parallel to the ground.

[9] TM mode waves are preferentially excited by vertical lightning currents [*Budden*, 1961, p. 61], i.e., CG lightning discharges, which tend to be vertical near the ground [*Krider et al.*, 1976], and the vertical portions of IC lightning discharges. Horizontal discharges, such as those found in IC lightning [*Krehbiel*, 1986], preferentially excite Transverse Electric (TE) mode waves [*Budden*, 1961, p. 64]. (It should also be noted that the excitation of TE waves from a horizontal source is dependent on the orientation of the source relative to the observer.) The orientation of the magnetic field of TE mode waves is perpendicular to the magnetic field of TM mode waves. Thus, the horizontal magnetic field component for TE waves is parallel to the overall direction of propagation through the waveguide. Therefore, the application of our technique to determine the arrival azimuth for sferics that are predominantly composed of TE mode waves would result in an error in azimuth of 90 degrees. Furthermore, for low order TE modes, the magnetic field is primarily vertical and therefore the magnitude of the detected sferic would appear smaller than that of an equally energetic TM mode sferic. Ninety degree errors in azimuth are actually seen in some of our data comparisons with the LIS, where as many as ~10% of LIS flashes are matched to sferics with an error in azimuth within 5° of 90°.

[10] In practice, sferics are not composed of idealized TM mode waves but are rather composed of a sum of quasi-TM (QTM) and quasi-TE (QTE) modes that deviate from ideal TM and TE modes due to the anisotropy of the ionosphere and the curvature of the Earth [*Martin*, 1965]. Also, higher order modes attenuate more rapidly than the lower order modes, thus, the lower order modes become more dominant as the distance from the source increases. Errors in the derived azimuth angle that are caused by deviations from ideal TM waves are typically referred to as polarization errors. *Yamashita and Sao* [1974a, 1974b] discuss in more detail some of the manifestations of polarization error, such as the effects of waveguide characteristics and of source polarization. Also, *Uman et al.* [1980] discusses errors caused by nonvertical lightning channels. In general, these errors are functions of frequency and decrease with increasing distance from the source or a local anisotropy or inhomogeneity. In this work, we assume polarization errors to be small based on the fact that at least one of the receiver sites are located at a large distance from most lightning sources. In addition, our method of averaging over a 4 kHz bandwidth tends to reduce the total polarization error since this type of error is frequency dependent. As mentioned previously, Vieques Island is unfortunately not at a large distance from all of the lightning sources studied, leading to significant polarization error when locating nearby (<1000 km) lightning.

[11] Error in the arrival azimuth calculation can also be caused by the properties of the receiver site. Appropriately referred to as "site error," this type of azimuth error is different for each site but the error is a calculable constant for any given azimuth and can therefore be removed in post-processing [*Mach et al.*, 1986]. The characteristic feature of site error is the presence of two cycle sinusoidal variations in error with respect to arrival azimuth [*Hiscox et al.*, 1984]. This variation is usually attributed to the topography of the surrounding terrain, such as nearby hills and elevation changes [*Horner*, 1954] or to nearby metallic objects and structures [*Hiscox et al.*, 1984; *Mach et al.*, 1986; *Passi and Lopez*, 1989], and is often minimized with some type of statistical algorithm. However, imperfections in the alignment and size of the two antennas can also cause a sinusoidal variation in azimuth error. The antennas of the type used in our study are imperfect in several ways. First, the north/south aligned antenna does not align perfectly with geographic north but is offset by some angle, ρ. Second, the antennas are not perfectly orthogonal but are skewed from orthogonality with respect to one another by some angle, ξ. Finally, the dimensions of the two loops may be different, resulting in different areas, which results in the induced voltage at the terminals of the antennas to be different for the same incident magnetic field intensity. The antenna response differences can be combined with any differences in system (i.e., in the preamplifier circuitry) gain to determine the total 'gain' of both the north/south and east/west channels. Using the geometry depicted in Figure 1, the azimuth error caused by imperfections in the dimensions of the antenna and its alignment can be corrected. Given a signal arriving from an azimuth, θ, the signals on the north/south and east/west channels are

$$S_{NS} = G_{NS}\cos(\theta - \rho) \tag{2}$$

$$S_{EW} = G_{EW}\sin(\theta - \rho - \xi), \tag{3}$$

where G_{NS} and G_{EW} are the gains of the north/south and east/west channels, respectively. Thus the calculated arrival azimuth θ_{calc}, is

$$\theta_{calc} = \arctan\left(\frac{S_{EW}}{S_{NS}}\right) = \arctan\left(\frac{G_{EW}}{G_{NS}}\frac{\sin(\theta - \rho - \xi)}{\cos(\theta - \rho)}\right). \tag{4}$$

Solving equation (4) for θ and substituting α for G_{NS}/G_{EW} yields the following equation for correcting site error caused by antenna imperfections:

$$\theta = \arctan\left[\alpha\frac{\tan(\theta_{calc})}{\cos(\xi)} + \tan(\xi)\right] + \rho. \tag{5}$$

The variables ρ, ξ and α vary from receiver site to receiver site and θ_{calc}, of course varies from event to event. Figure 2

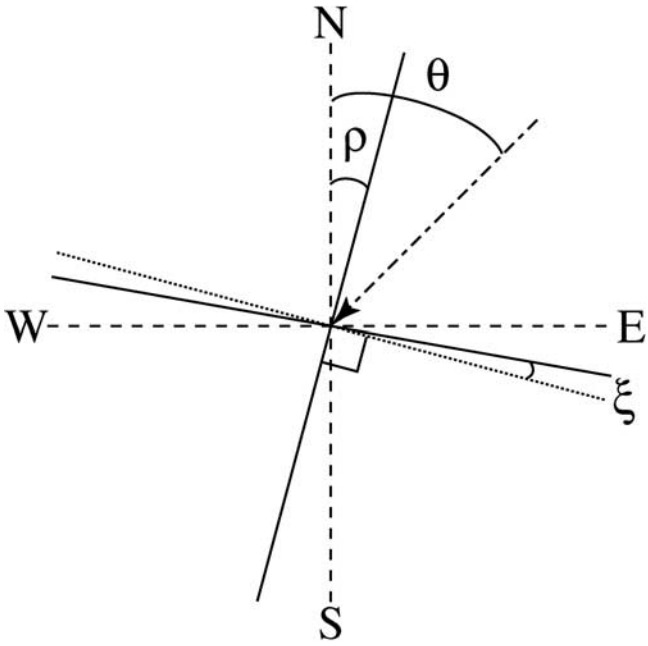

Figure 1. Magnetic Loop Antenna Geometry, where ρ is the deviation of the NS antenna from due north, ξ is the skew of the two antennas relative to orthogonal and θ is the arrival azimuth of an incoming sferic.

shows a histogram of the arrival azimuth error (after correction for site errors) for 2771 sferics that were detected at Palmer Station, Antarctica and matched to NLDN lightning flashes [*Wood and Inan*, 2002]. The overlying curve in Figure 2 is a Gaussian with a mean of 0 and standard deviation of 1. The high degree of correlation between the curve and the histogram suggests the error is dominantly random in nature and that the direction finding method is thus quite effective upon subtraction of the systematic site errors. The parameters used for Palmer Station, as determined by measurements taken at the site and comparison with expected NLDN and VLF transmitter arrival azimuths, are $\rho = 4.0°$, $\xi = 2.4°$ and $\alpha = 0.90$. Figure 3 shows a similar histogram for sferics detected at Vieques Island on 08 September 2001. On this day, 8363 sferics detected at Vieques were matched to NLDN lightning flashes. The overlying curve is once again a Gaussian with mean of 0 and standard deviation of 1. As is apparent in this figure, the error distribution does not quite match the curve but rather has "side lobes" of larger errors. These errors are probably due to increased polarization error due to the closer proximity of the site to the lightning sources. The parameters used for Vieques Island are $\rho = -7.0°$, $\xi = -4.0°$ and $\alpha = 0.75$. For more details about the determination of the arrival azimuths please refer to *Wood and Inan* [2002].

[12] Furthermore, for the Palmer Station site, the minimum field strength amplitude for which the azimuth of a sferic can be correctly determined (within 5°) is ~250 μV/m. This roughly corresponds to the detection of a lightning discharge with a peak current of ~10 kA at a range of ~10,000 km. For the Vieques Island site, the minimum required amplitude is about 25 mV/m, which roughly corresponds to the detection of a ~10 kA lightning discharge at a range of ~3,500 km. This higher threshold of detection limits the system to locating lightning primarily in North and South America, although, some of the very largest flashes from Africa are also detected. However, the number of flashes detected in Africa is overshadowed by the number of flashes detected in South America. Therefore, in this study, we focus our attention on the detection and location of lightning in South America.

[13] Once the arrival azimuths at the two receiver sites are calculated, the locations of lightning sources can be determined via spherical triangulation. The first panel in Figure 4 shows lines of azimuth originating from Palmer Station, indicated by the solid lines, and Vieques Island, indicated by the dashed lines. The lines of azimuth from the two sites

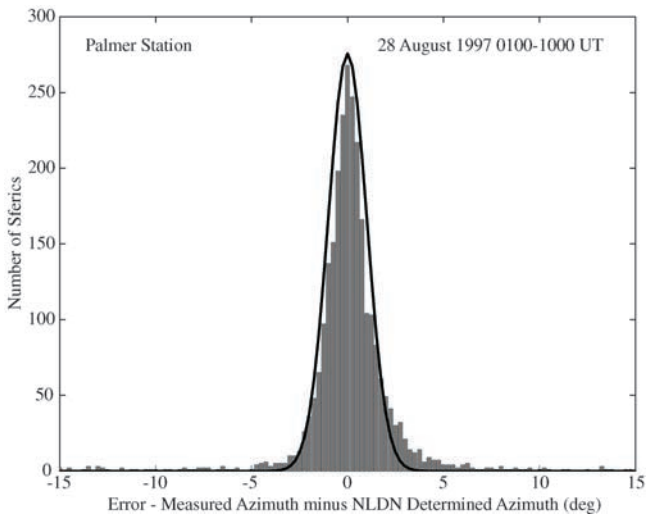

Figure 2. Histogram of arrival azimuth error for sferics detected at Palmer Station, Antarctica, from 0100–1000 UT on 28 August 1997. 2771 sferics were matched to NLDN flashes.

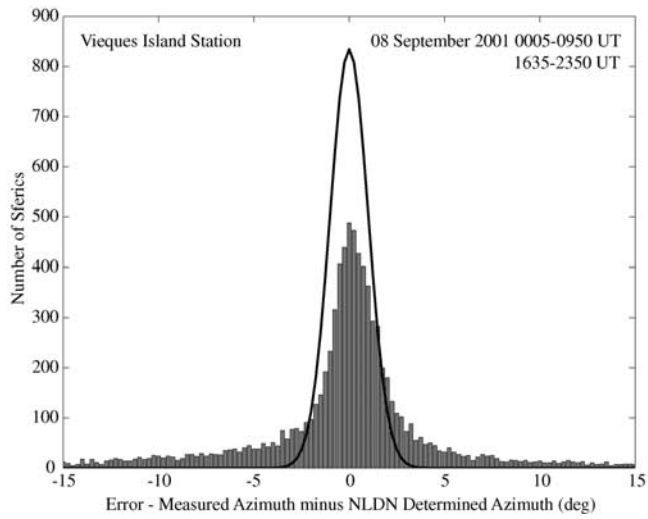

Figure 3. Histogram of arrival azimuth error for sferics detected at Vieques Island, Puerto Rico, from 0000–1000 UT and 1630–2400 UT on September 8, 2001. 8363 sferics were matched to NLDN flashes.

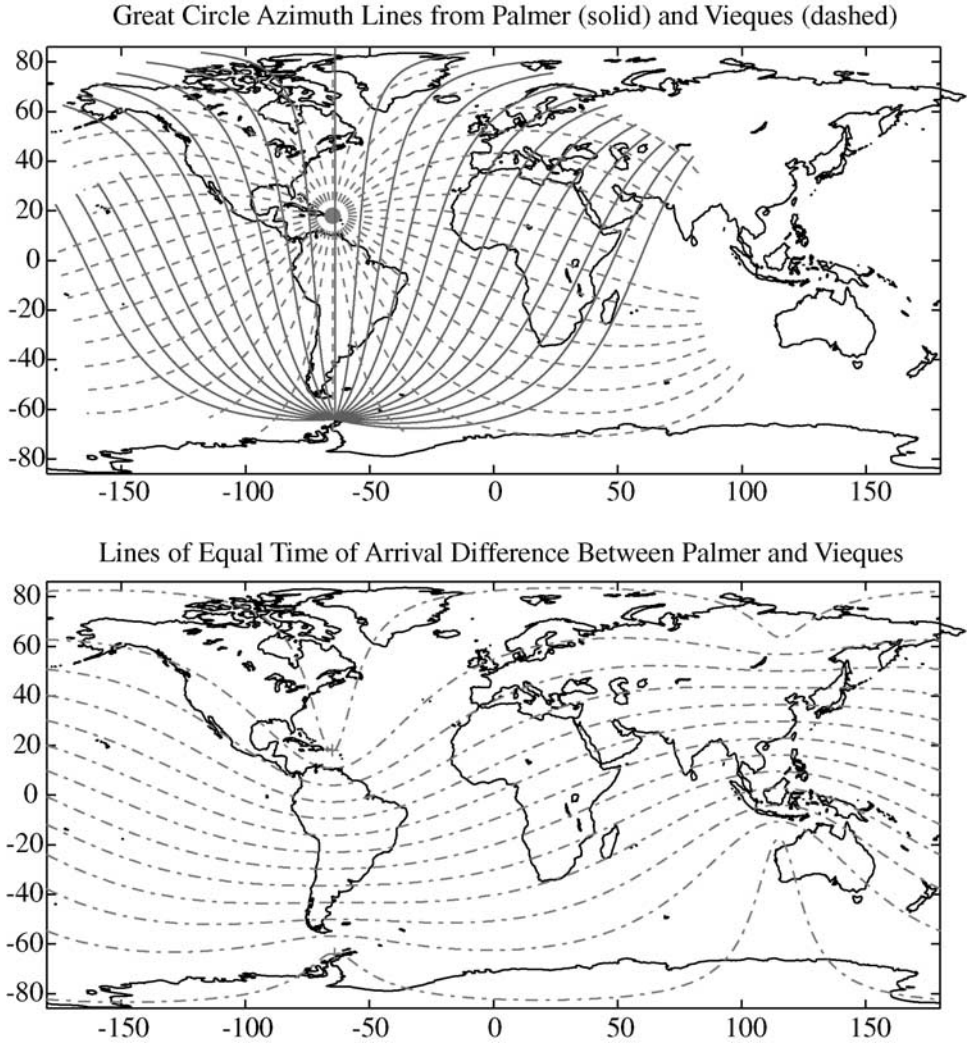

Figure 4. Lines of azimuth from Palmer Station, Antarctica (solid lines), and Vieques Island, Puerto Rico (dashed lines) (upper). Line of equal time of arrival difference between Palmer Station and Vieques Island. (lower) Lines are spaced at 5 ms intervals.

form a grid that can be used to triangulate the source location of a lightning discharge. Given a site location and an arrival azimuth, a great circle path is defined about the Earth. These great circle paths are equivalent to the meridians of longitude if the receiver sites are located at the north or south poles. Also, any two distinct great circle paths intersect each other at exactly two points, which can be determined using spherical trigonometry [*Orville*, 1987]. Therefore sferic arrival azimuths from Palmer Station and Vieques Island that come from the same lightning discharge provide coordinates for two points on the Earth, which are antipodal to each other. The points of intersection determined by the arrival azimuths serve as a starting point for our determination of the source locations of lightning discharges.

[14] In the absence of errors in arrival azimuth measurements, one of the two points of intersection between the great circle paths would be the source location for the lightning discharge. However, errors are, in practice, present in the azimuth measurements and translate into errors in the location estimate. This error is a minimum when the great circle paths from the two sites cross one another at angles near 90 degrees and a maximum when great circle paths are close to parallel, which is the case for source locations along or near the great circle path connecting the two receiver sites. For such source locations, a small error in azimuth has a large effect on the points of intersection of the two great circle paths. In order to find a better estimate for the lightning source location, the difference in the time of arrival (TOA) for the sferics at the two receivers is incorporated into the location algorithm.

[15] The bottom panel of Figure 4 shows lines of equal TOA difference between Palmer Station and Vieques Island. Assuming uniform propagation velocity, sferics originating on the same line have equal TOA differences between Palmer Station and Vieques Island. When a line of equal TOA difference is combined with arrival azimuth lines from Palmer Station and Vieques Island, a set of quasi-spherical triangles are created. They are quasi-spherical since the lines of equal TOA difference are spherical hyperbolas and not great circles. Figure 5 shows the geometry that might develop from measurements taken from a sferic originating

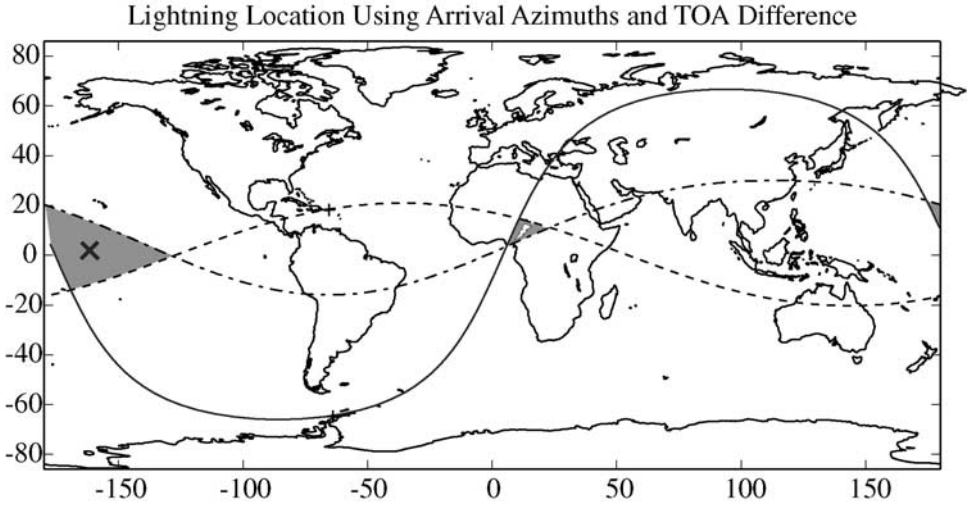

Figure 5. Example two station lightning location for a lightning discharge occurring in central Africa. The solid line is the azimuth from Palmer Station. The dashed line is the azimuth from Vieques Island. The dot-dashed line is the line of equal time of arrival difference. These lines form triangles (shaded) on the Earth, with the smaller triangle the most likely location for the lightning strike.

in central Africa. The solid line is the arrival azimuth at Palmer Station, the dashed line is the arrival azimuth at Vieques Island while the dot-dashed line represents equal TOA difference. These lines form a small triangle at one location, in this case Africa, but also form another (larger) triangle on the other side of the Earth. The geometry in Figure 5 shows the triangle enclosing the actual lightning event although statistically this does not have to be the case.

[16] As an analytical solution, the gravity center of this triangle was suggested by *Sato and Fukunishi* [2003], but a numerical method is used here instead. For every point (with 25 km resolution in latitude and longitude) on the surface of the Earth the expected values for the arrival azimuths at Palmer Station and Vieques Island from that point and the expected TOA difference to the two stations are first computed. These values are then put into a look-up table for future use. When performing a triangulation, the points of intersection of the two arrival azimuths are used as starting points. (Thus the location estimation is performed at both intersection points.) At each point and its eight surrounding points (see Figure 6) the residual error is computed using the chi-square function

$$\chi^2 = c_1\left(az_{pa} - az_{pa\_ideal}\right)^2 + c_2(az_{vi} - az_{vi\_ideal})^2 + c_3(toa_{ms} - toa_{ms\_ideal})^2, \quad (6)$$

where az_{pa} is the measured arrival azimuth at Palmer Station, az_{pa_ideal} is the pre-calculated Palmer Station arrival azimuth, az_{vi} is the measured arrival azimuth at Vieques Island, az_{vi_ideal} is the pre-calculated Vieques Island azimuth, toa_{ms} is the measure TOA difference in milliseconds and toa_{ms_ideal} is the pre-calculated TOA difference in milliseconds. The values c_1, c_2 and c_3 determine the weighting of each measurement. Any chi-square function can be used but the measurement with the least expected error should have the highest weighting [*Hiscox et al.*, 1984]. In our study, c_1 and c_2 are given a weighting of 1 and c_3 is given a weighting of 4 since the standard deviation in azimuth error is one degree and the standard deviation in the timing error, when matched to NLDN times, is about half a millisecond. It may at first be questioned as to whether it is appropriate to combine measurements of quantities with different units in this manner. However, each component in the chi-square function should be thought of in terms of its correspondence to the same position error at a range of 5,000–10,000 km.

[17] After computing the chi-square function at all nine points, we determine whether one of the eight points surrounding the intersection point has a smaller chi-square error than the intersection point, and if so use that point as the new starting point. Once again the chi-square function at all of the surrounding points is computed and the process is

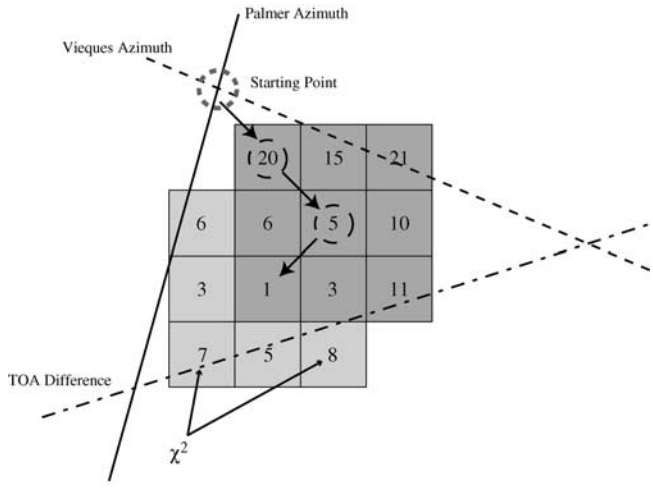

Figure 6. Cartoon showing how the location optimization occurs using a look-up table. The starting point for the look-up process is at the intersection of the two azimuth lines. The values in the squares represent the output of the chi-square error function. In this example the lightning source location estimate is in the square with a chi-square error of 1.

continued until the minimum chi-square error point is reached. Figure 6 illustrates how the minimum chi-square error point is found by ''sliding'' down the chi-square error gradient. Once again, since the azimuth lines intersect at two points, this process is performed at both points. Thus two minima are found on opposite sides of the Earth. The first criterion for selecting one of the two points as the most likely point is to make sure the point falls within range of the receivers, deemed to be about 10,000 kilometers. If both points are within range of both of the receivers then the point with the smallest chi-square error, corresponding to the point inside of the smallest triangle, is selected.

[18] Because the two receivers are widely separated, a space-time complication arises when attempting to match sferics received at one site with the corresponding sferics received at another site. Since the global flash rate is as high as 100 flashes every second [*Orville and Spencer*, 1979], it is sometimes ambiguous as to which sferics match to one another. This is, in part, due to the high sferic rate at Palmer Station, which can be upwards of 100 per second (obviously not all sferics from around the world are detectable at Palmer Station but most flashes generate multiple sferics). As an example, a lightning discharge A occurring close to one receiver may be followed a few milliseconds later by a lightning discharge B occurring close to the other site. In such a circumstance, the sferic from discharge A arrives at the first receiver followed by the sferic from discharge B. However, at the second receiver, the sferic from discharge B arrives first, followed by the sferic from discharge A. To account for this possibility, triangulation is performed on all possible sferic matches. In other words, given a sferic arrival time at one site, triangulation is performed by pairing this sferic with all sferics arriving at the other site during the allowable time frame. For the particular two sites of concern for this paper, the time frame is plus or minus 30 milliseconds, which is the propagation time from one receiver to another over a distance of 9130 km. It is impossible for a sferic coming from a unique lightning source to have an ATD greater than this. After all of the triangulations are performed the best-best source location is selected based on the triangulation which has the smallest chi-square error value. Also, a maximum chi-square error threshold is set for reporting an event location as is discussed in the simulation results.

3. Simulation Results

[19] Before application of the technique described above on actual data it is useful to simulate the conditions under which the algorithm is to be used. Simulation provides information about three types of error that occur in the use of such an algorithm. The most obvious type of error is the location accuracy by which individual lightning discharges can be determined. The upper left panel of Figure 7 shows results for simulated discharges occurring at: a, (30°N latitude, 100°W longitude); b, (5°N, 0°); c, (10°S, 75°W); d, (25°S, 65°W); e, (35°N, 65°W). Locations a and b were chosen to show the performance of the system near the extreme of its range. Locations c and d were chosen to show the optimal performance region for the system, while location e was chosen to show the least optimal performance region. For the simulation, we first calculate the expected arrival azimuths and arrival times at Palmer Station and Vieques Island. A random error with mean 0 and standard deviation of 1° is then added to each of these calculations, in accordance with the expected measurement error as shown in Figure 2. We assume the same for the Vieques site since we are interested in the sferics arriving from an appropriately long range. The expected TOA difference is also calculated and a time error with a 0 millisecond mean and a half millisecond standard deviation was added. The simulated sferic measurements are then given as inputs to the triangulation and location determination algorithm. The median error for the discharge at location a is ~110 kilometers and the median error for the discharge at location b is ~105 kilometers. The smallest errors occur for the locations in South America, c and d, which have median errors of ~75 kilometers, while the largest error occurs at location e which has a median location error of ~2000 kilometers. For all cases the black crosses identify the location where the event occurred and the gray area spans the region within which the simulated events were located. Simulation results also show that the more accurate the azimuth and time of arrival measurements, the lower are standard deviations, and the location errors. For example, doubling the standard deviation of all of your measurements doubles the location error and vice versa.

[20] The second kind of error present in the simulations, shown in the upper right panel of Figure 7, occurs when the algorithm mistakenly places the discharge location at the antipodal point of its actual location. For a two receiver array, there are certain regions where the grid formed by the azimuth lines and TOA difference lines is symmetric and the azimuth lines and the time of arrival difference line converge equally at antipodal points on the Earth. When error is added to the measurements, the minimum error point can switch from the correct position to the antipodal position. One of these sensitive regions is located at the center of the array between the two receiver sites. Fortunately, this region does not pose a problem since, with the two sites both being in the western hemisphere and at about the same longitude, it is highly unlikely that a sferic generated by a lightning strike on the opposite side of the Earth (which corresponds to the Indian subcontinent) would be detected by the receivers due simply to the very long distances (and thus high attenuations) involved. Therefore, the location between the receiver sites is always selected even if the antipodal point has lower error. The other region of concern, shown in the upper right panel of Figure 7, is unfortunately located in Central Africa, one of the most lightning active regions in the world [*Boccippio et al.*, 2002]. In Figure 7, we see that many of the simulated lightning discharges are shown (gray colored area) to be incorrectly located near the antipodal point of Central Africa, which is in the middle of the Pacific Ocean.

[21] The third kind of error revealed in the simulations is caused by the ambiguous matching of sferics detected at one receiver site to those detected at the other receiver site. This error is referred to as ''mismatch'' error. For this simulation, virtual storms were created at (15°N, 95°W) and (10°N, 75°W), designated respectively as storm A and storm B. Each storm was set to produce lightning discharges at

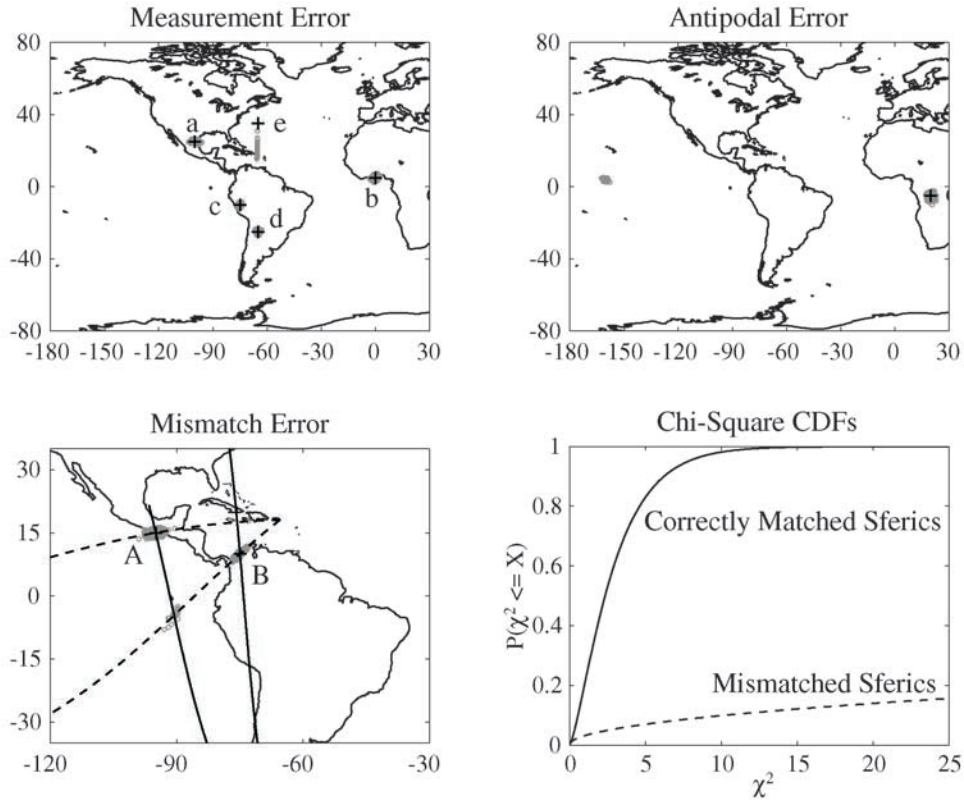

Figure 7. The upper left panel shows the measurement error for lightning locations at points a, b, c, d, and e. The locations are given by the black pluses, and the gray areas show the span of where the algorithm will locate the strike. The upper right panel shows a case of antipodal error. In this case the lighting strike, shown by the plus, is sometimes mistakenly located on the opposite side of the Earth. The lower left panel shows mismatch error in located sferics. In some cases the sferics from storm A are mismatched to sferics from storm B resulting in sferics being incorrectly located at the crossing point of the solid and dashed lines. The bottom right panel shows the CDFs for the chi-square error for correctly matched sferics and mismatched sferics. Correctly matched sferics should have a chi-square error of less than 13.

random times with an inter-discharge interval specified by the exponential distribution

$$f_T(t) = \lambda_1 e^{-\lambda_1 t}, t \geq 0 \tag{7}$$

with $\lambda_1 = 12.76\ s^{-1}$ [*Chrissan*, 1998, pp. 51–68]. The results of this simulation are shown in the bottom right panel of Figure 7 along with the arrival azimuth lines from Palmer Station (solid lines) and Vieques Island (dashed lines). The majority of the lightning dicharges are located correctly to within the expected position error, ~100 km, determined by the measurement accuracy. However, a few discharges are incorrectly located at the crossing point of two "mismatched" azimuth lines. This type of mismatching occurs when a sferic from storm A detected at Palmer Station is matched to a sferic from storm B detected at Vieques Island. In order for the discharge to be incorrectly located at the crossing point of these azimuth lines, the error value for the mismatched sferics must be less than the error value that exists when the Palmer Station sferic is correctly matched to its corresponding Vieques Island sferic. Such a condition occurs by chance even though they are unrelated events, in those cases when the time of arrival difference between mismatched sferics happens to be low.

[22] The lower right panel of Figure 7 shows the cumulative density functions (CDF) for the chi-square error function for correctly matched sferics (solid line) and mismatched sferics (dashed line). It is evident that almost 100% of correctly matched sferics have a chi-square error value of 13 or less, while only about 10% of mismatched sferics have a chi-square error of 13 or less. However, in some cases the chi-square value for mismatched sferics might be lower than the chi-square value for correctly matched sferics. When this occurs, some lightning discharges are incorrectly located, as is revealed in the lower left panel of Figure 7 by the gray circles located out in the middle of the Pacific Ocean. These errors occur primarily due to the high sensitivity of the receivers used, which can detect sferics arriving from over 10,000 kilometers away, so that the flash rate seen by a single receiver is the sum total of the flash rates for all the storms within 10,000 kilometers.

4. Application to Real Lightning Data

[23] Due to the synoptic (i.e., 1-min out of every 15-min) style recording schedule and occasional system failures at the Vieques Island receiver site, the practical performance of the triangulation algorithm is best judged by comparison to

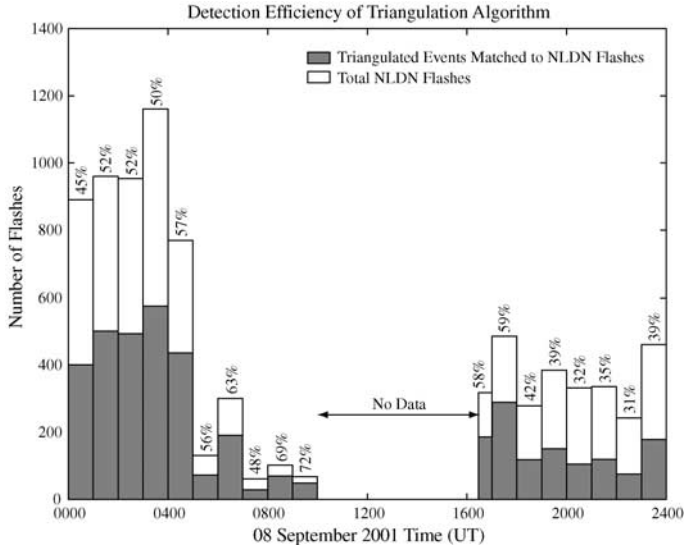

Figure 8. The detection efficiency for detecting NLDN flashes versus the time of day for data acquired on 8 September 2001. Detection efficiency is highest between 0900–1000 UT and lowest between 2200–2300 UT.

the NLDN (the data for which are continuously available), rather than TRMM/LIS data which views a given area for only a short duration each day. Figure 8 shows the detection efficiency relative to the NLDN detected cloud-to-ground flashes for 8 September 2001. The top of each white bar is the total number of NLDN flashes that occur during the periods for which Vieques Island and Palmer Station data are available. The top of each gray bar is the number of those NLDN flashes that were matched to triangulated events. A triangulated event is considered a match if it occurrs within 2 milliseconds of an NLDN flash time and within 750 kilometers of the NLDN location. The highest detection efficiency is found during the 0900–1000 UT time period where 72% of NLDN flashes are detected. The lowest detection efficiency is found during the 2200–2300 UT time period where only 31% of NLDN flashes are detected. This is consistent with the fact that VLF signals are subject to lower attenuation at night than during the day. Overall, for the entire day, 49% of NLDN flashes are detected. Once again, no data are available during the 1000–1630 UT time period, due to spotty recording schedule at Vieques.

[24] Figure 9 shows the location accuracy of the 8 September 2001 triangulated events that are matched to NLDN flashes. The smallest location error is found during the 0000–0100 UT time period where the median location error is 174 km. The greatest location error is found during the 1900–2000 UT time period where the median error is 298 km. Also, the 0000–1000 UT time period shows slightly better performance than the 1630–2400 UT time period. The 0000–1000 UT time period corresponds to nighttime propagation conditions from North America to the two receiver sites and the 1630–2400 corresponds to daytime propagation conditions. The difference in location error may also be due to the location of the lightning strikes in North America, as strikes occurring in the eastern United States will have poorer location performance than strikes occurring in the western United States due to the relative locations of the receivers.

[25] A general comparison of areas of lighting activity can be made with the Lightning Imaging Sensor (LIS) aboard the Tropical Rainfall Measurement Mission (TRMM) satellite. The upper panel of Figure 10 shows the sum of all lightning events located by LIS from 0000–2400 UT on 9 September 2001. Due to its low Earth orbit, the TRMM satellite only passes over a particular area at certain times during the day. For example on 9 September 2001, Florida is over flown at about 1140 UT and 1630 UT. The remaining panels of Figure 10 show lightning locations determined using the technique introduced in this paper with data from Palmer Station and Vieques Island. The bottom four panels show lightning locations from 0000–0300 UT, 0700–1000 UT, 1600–1900 UT and 2000–2300 UT on 9 September 2001. These time periods were selected to show how lightning activity varies over the

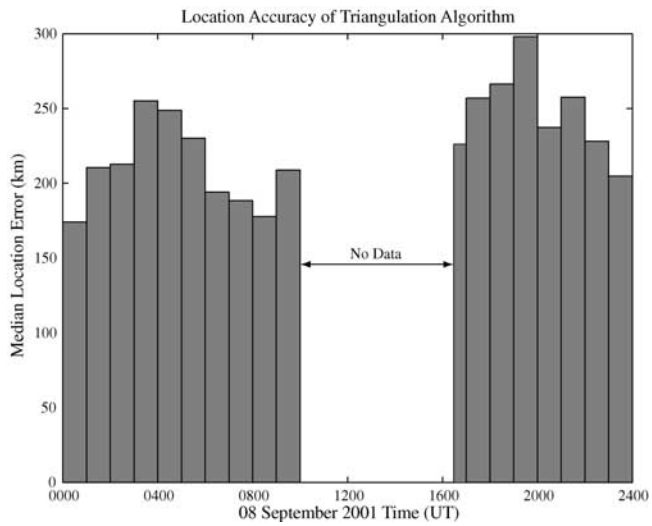

Figure 9. Location accuracy for the detection of NLDN events versus time of day for 8 September 2001. The median location error for the entire day is about 200 km.

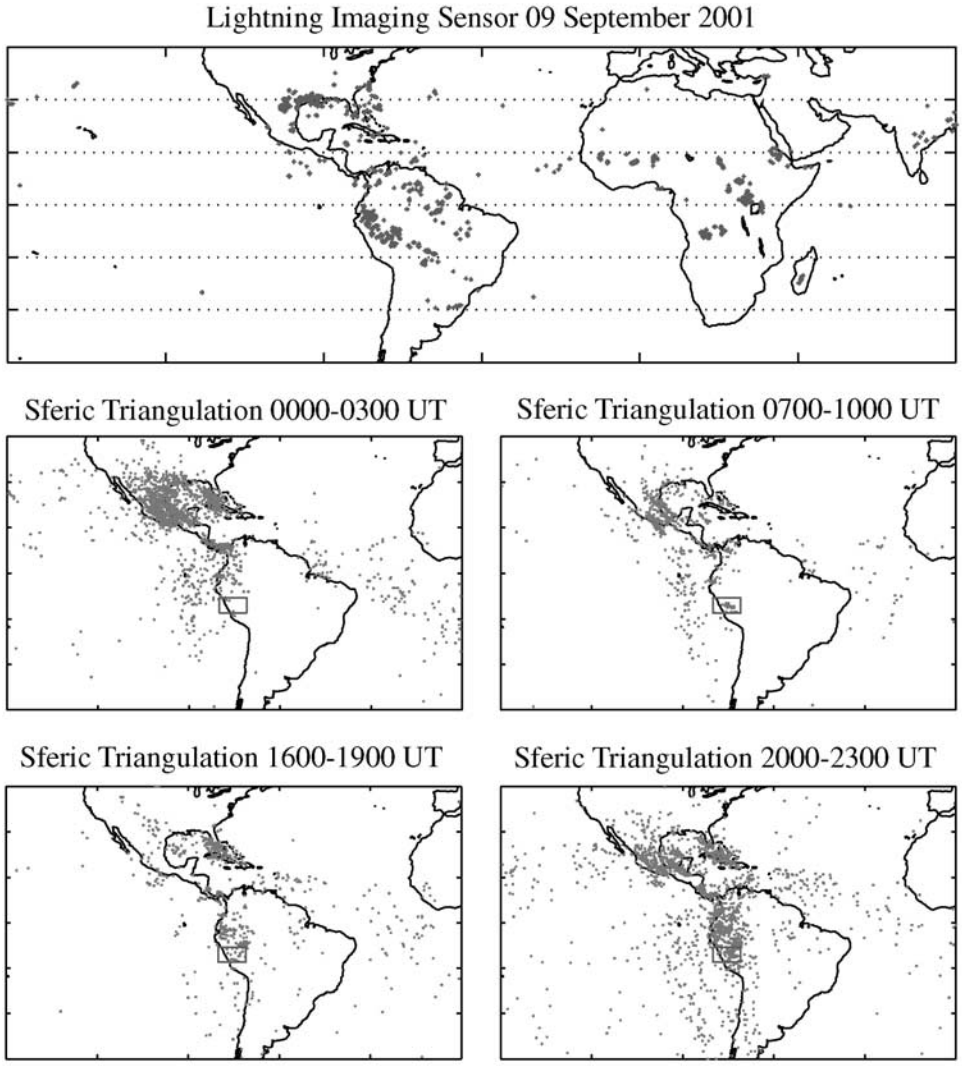

Figure 10. Comparison between lightning events detected using two station lightning location and lightning events detected by the Lightning Imaging Sensor on 9 September 2001.

course of the day in different regions. For example, during the 0000–0300 UT period there is a lot of lightning activity in and around Mexico. This activity is not visible in the LIS data because the LIS passes over Mexico occurred later in the day at around 1200 UT and 1800 UT. However, the minimal lightning activity around Mexico in the LIS data around 1800 UT is consistent with the panel showing the triangulated lightning from 1600–1900 UT. Mismatch errors are also visible in the triangulated lightning data off the west coast of South America. Notice that more mismatch errors, seen as an increase in number of scattered non-clustered events, occur during times of increased lightning activity such as during the 0000–0300 UT and 2000–2300 UT time periods. In contrast, fewer mismatch errors occur during periods of less lightning activity such as the 0700–1000 UT and 1600–1900 UT time periods.

[26] Once again, due to the synoptic style recording scheme and the occasional system failures at the Vieques Island receiver site, it is difficult to find LIS passes that were in range of the receivers while data were being recorded. However, one pass over South America occurred for which performance statistics could be derived. At 0550 UT on 10 September 2001 the LIS instrument passed over the point near 11°S latitude and 72°W longitude. During this time, the LIS detected 121 flashes. Of these flashes, 25, or 21% of the flashes, are matched within 2 milliseconds of an event located by the triangulation algorithm. The matches are made to the time of the largest "group" in each LIS flash. The median location error for the 25 matched events is 188 kilometers which is about a factor of two worse than the expected median error for this region, 75 kilometers, as predicted by simulation.

[27] The triangulation technique described above can also be used to continuously monitor a particular area over the course of several days. In Figure 10, the rectangle visible in South America spans the area from 8°S to 13°S and from 71°W to 80°W. This area was selected because a localized cluster of events is often visible here in the data without a lot of extraneous, possible erroneous, events around it. Thus it is hoped that the event rate for this area can be studied without the inclusion of erroneously located or mismatched events. This area also contains the region for which LIS data

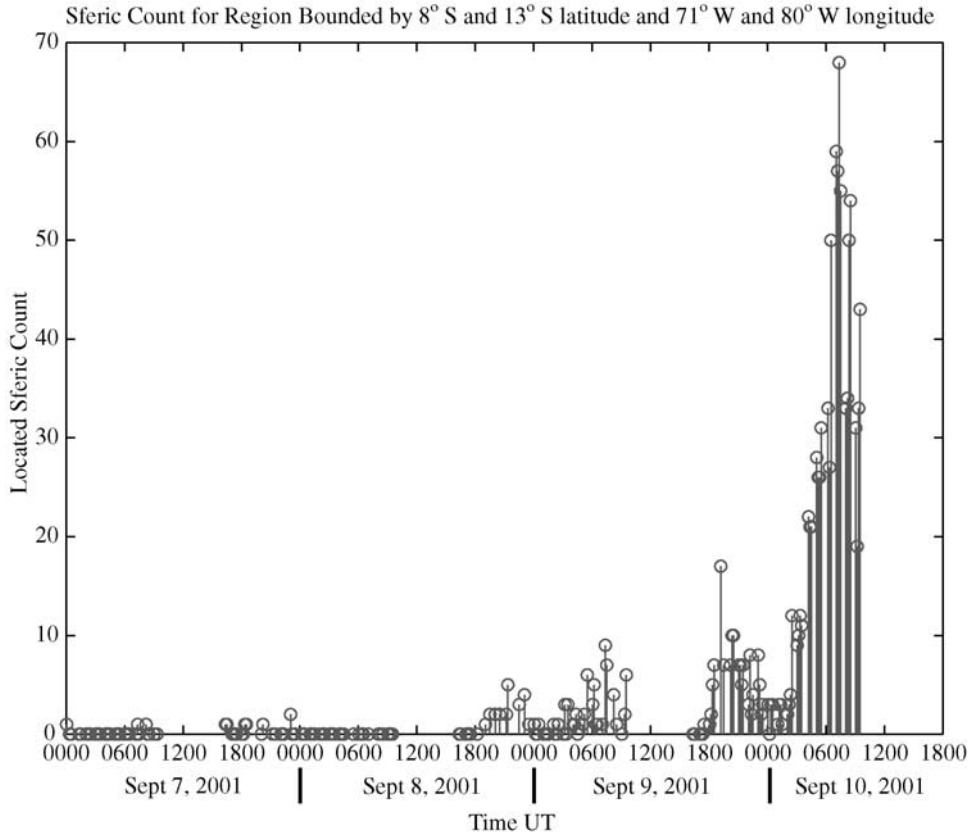

Figure 11. Sferic localization rate for a localized storm in South America. The sferic rate from region displays a high level of correlation from one day to the next.

were matched to triangulated events. In conjunction with another experiment, data were acquired at both Palmer Station and Vieques Island from 0000–1000 UT and 1630–2400 UT over the course of several days. No data were collected from 1000–1630 UT because the Arecibo radio telescope, which was being used as part of the other experiment, was not available during this time. The data were acquired for one-minute intervals at 5, 20, 35 and 50 minutes past each hour. This synoptic recording schedule was used because the system had limited storage capacity and had to operate autonomously for several days. Furthermore, some of these synoptic data files were corrupted and not suitable for analysis. For each minute interval the sferics with triangulated locations falling within the rectangular area were counted. Figure 11 shows the sferic counts from 0000 UT on September 7, 2001 to 1000 UT on September 10, 2001. Initially, for the first 46 hours of observation, very few events are located within the area of interest. However, subsequently there is a noticeable increase in event occurrence during the synoptic periods over the next 16 hours. There is then an even more remarkable increase in the event occurrence rate during the next 24 hours after that. The highest event rate occurs at 0705 UT on 10 September 10th with 68 sferics located in the boxed area during this minute.

[28] Also of interest in Figure 11 is the daily cycle of sferic occurrence that is visible during the final 40 hours of observation. Starting at 1800 UT on September 8th there is a lull in the event occurrence rate. The lull is followed in time by a small peak in the event rate that occurs at approximately 2100 UT. This peak is in turn followed by another lull at approximately 0130 UT and is then followed by a larger peak 0700 UT. Coincidentally this exact same pattern of lulls and peaks is repeated again starting at 1800 UT on September 9th except that this time the magnitude of the peaks are larger. Unfortunately, data are not available during the next 24 hours in order to see if this pattern repeats again. This daily variation in sferic occurrence is similar to the daily electric field variations seen aboard the HMS Carnegie during its voyage [*Chalmers*, 1967] in that the variation appears to repeat over a 24-hour period. However, the double peak is inconsistent with the so-called Carnegie curve. Similar diurnal variations in lightning activity were also seen by *Zajac and Rutledge* [2001] in North America and by *Pinto et al.* [1999] in Brazil.

5. Summary

[29] We have demonstrated that the sources for sferics can be located using two receivers separated by global distances. The two receivers used in this example were located at Palmer Station, Antarctica and Vieques Island, Puerto Rico. Using a combined magnetic direction finding and time of arrival difference technique, lightning discharges were located in North America and South America. For the discharges in North America, 49% of the cloud-to-ground flashes detected by the National Lightning Detection Network were located by the triangulation algorithm with a median location error of ~200 kilometers. For discharges

in South America, 21% of the flashes detected by the Lightning Imaging Sensor during one of its passes were located by the triangulation algorithm with a median error of 188 kilometers. Since lightning discharges can be located at such large distances, a limited number of receiver locations would be needed to cover the entire Earth. Furthermore, if the sferic from a lightning strike is visible at more than two receiver sites then the location accuracy should increase since, for example, detection by three sites would provide six measurements (three directions and three TOA differences) while detection by two sites only provides three measurements (two directions and one TOA difference).

[30] **Acknowledgments.** This research was supported by the National Science Foundation under grants OPP-9910565 and OPP-0233955. T. Wood was partially supported (earlier in this work) by NASA under grant NGT 5-50227. NLDN data provided by the NASA Lightning Imaging Sensor (LIS) instrument team and the LIS data center via the Global Hydrology Resource Center (GHRC) located at the Global Hydrology and Climate Center (GHCC), Huntsville, Alabama, through a license agreement with Global Atmospherics, Inc. (GAI). The data available from the GHRC are restricted to LIS science team collaborators and to NASA EOS and TRMM investigators. Special thanks to Ken Cummins of Global Atmospherics, now Vaisala, for information on the NLDN and to Victor Pasko at Penn State University.

References

Alexander, G. D., J. A. Weinman, V. M. Karyampudi, W. S. Olson, and A. C. L. Lee (1999), The effect of assimilating rain rates derived from satellites and lightning on forecasts of the 1993 superstorm, *Mon. Weather Rev.*, *127*, 1433–1457.

Baker, M. B., H. J. Christian, and J. Latham (1995), A computational study of the relationships linking lightning frequency, and other thundercloud parameters, *Q. J. R. Meteorol. Soc.*, *121*, 1525–1548.

Baker, M. B., A. M. Blyth, H. J. Christian, J. Latham, K. L. Miller, and A. M. Gadian (1999), Relationships between lightning activity and various thundercloud parameters: Satellite and modeling studies, *J. Atmos. Res.*, *51*, 221–236.

Boccippio, D. J., S. J. Goodman, and S. Heckman (2000), Regional differences in tropical lightning distributions, *J. Appl. Meteorol.*, *39*, 2231–2248.

Boccippio, D. J., W. J. Koshak, and R. J. Blakeslee (2002), Performance assessment of the Optical Transient Detector and Lightning Imaging Sensor: 1. Predicted diurnal variability, *J. Atmos. Oceanic Technol.*, *19*, 1318–1332.

Budden, K. G. (1961), *The Wave-Guide Mode Theory of Wave Propagation*, Logos, London.

Burke, C. P., and D. L. Jones (1995), Global radiolocation in the lower ELF frequency band, *J. Geophys. Res.*, *100*, 26,263–26,271.

Chalmers, J. A. (1967), *Atmospheric Electricity*, Pergamon, New York.

Cherna, E. V., and E. J. Stansbury (1986), Sferic rate in relation to thunderstorm dimensions, *J. Geophys. Res.*, *91*, 8701–8707.

Chrissan, D. (1998), Statistical analysis and modeling of low-frequency radio noise and improvement of low-frequency communications, Ph.D. thesis, Stanford Univ., Stanford, Calif.

Christian, H. J., et al. (1999), The lightning imaging sensor, paper presented at 11th International Conference on Atmospheric Electricity, NASA, Gunthersville, Ala.

Christian, H. J., et al. (2003), Global frequency and distribution of lightning as observed from space by the Optical Transient Detector, *J. Geophys. Res.*, *108*(D1), 4005, doi:10.1029/2002JD002347.

Cummins, K. L., M. J. Murphy, E. A. Bardo, W. L. Hiscox, R. B. Pyle, and A. E. Pifer (1998), A comibined TOA/MDF technology upgrade of the U.S. National Lightning Detection Network, *J. Geophys. Res.*, *103*, 9035–9044.

Davies, K. (1965), Ionospheric radio propagation, U.S. Dep. of Commun., Natl. Bur. of Stand., Gaithersburg, Md.

Dowden, R. L., J. B. Brundell, and C. J. Rodger (2002), VLF lightning location by time of group arrival (TOGA) at multiple sites, *J. Atmos. Sol. Terr. Phys.*, *64*, 817–830.

Fullerkrug, M., and S. Constable (2000), Global triangulation of intense lightning discharges, *Geophys. Res. Lett.*, *27*, 333–336.

Grosh, R. C. (1978), Lightning and precipitation—The life history of isolated thunderstorms, paper presented at Conference on Cloud Physics and Atmospheric Electricity, Am. Meteorol. Soc., Issaquah, Wash.

Hiscox, W. L., E. P. Krider, A. E. Pifer, and M. A. Uman (1984), A systematic method for identifying and correcting "site errors" in a network of magnetic direction finders, paper presented at International Aerospace and Ground Conference on Lightning and Static Electricity, Natl. Interagency Coord. Group, Natl. Atmos. Electr. Hazard Program, Orlando, Fla., 26–28 June.

Horner, F. (1954), The accuracy of the location of sources of atmospherics by radio direction-finding, *Proc. Inst. Electr. Eng.*, *101*, 383–390.

Huang, E., E. Williams, R. Boldi, S. Heckman, W. Lyons, M. Taylor, T. Nelson, and C. Wong (1999), Criteria for sprites and elves based on Schumann resonance observations, *J. Geophys. Res.*, *104*, 16,943–16,964.

Hughes, H. G., and R. J. Gallenberger (1974), Propagation of extremely low-frequency (ELF) atmospherics over a mixed day-night path, *J. Atmos. Terr. Phys.*, *36*, 1643–1661.

Kempf, N. M., and E. P. Krider (2003), Cloud-to-ground lightning and surface rainfall during the Great Flood of 1993, *Mon. Weather Rev.*, *131*, 1140–1149.

Krehbiel, P. R. (1986), The electrical structure of thunderstorms, in *The Earth's Electrical Environment*, pp. 90–113, Natl. Acad., Washington, D. C.

Krider, E. P., R. C. Noggle, and M. A. Uman (1976), A gated, wideband magnetic direction finder for lightning return strokes, *J. Appl. Meteorol.*, *15*, 301–306.

Lee, A. C. L. (1986), An experimental study on the remote location of lightning flashes using a VLF arrival time difference technique, *Q. J. R. Meteorol. Soc.*, *112*, 203–229.

Lee, A. C. L. (1990), Bias elimination and scatter in lightning location by the VLF arrival time difference technique, *J. Atmos. Oceanic Technol.*, *7*, 719–733.

Lewis, E. A., R. B. Harvey, and J. E. Rasmussen (1960), Hyperbolic direction finding with sferics of transatlantic origin, *J. Geophys. Res.*, *65*, 1879–1905.

MacGorman, D. R., D. W. Burgess, V. Mazur, W. D. Rust, W. L. Taylor, and B. C. Johnson (1989), Lightning rates relative to tornadic storm evolution on 22 May 1981, *J. Atmos. Sci.*, *46*, 221–250.

Mach, D. M., D. R. MacGorman, and W. D. Rust (1986), Site errors and detection efficiency in a magnetic direction-finder network for locating lightning strikes to ground, *J. Atmos. Oceanic Technol.*, *3*, 67–74.

Martin, H. G. (1965), The polarization of low frequency radio waves in the terrestrial wave-guide, *J. Atmos. Terr. Phys.*, *27*, 995–1007.

Orville, R. E., Jr. (1987), An analytical solution to obtain the optimum source location using multiple direction finders on a spherical surface, *J. Geophys. Res.*, *92*, 10,877–10,886.

Orville, R. E., and D. W. Spencer (1979), Global lightning flash frequency, *Mon. Weather Rev.*, *107*, 934–943.

Passi, R. M., and R. E. Lopez (1989), A parametric estimation of systematic errors in networks of magnetic direction finders, *J. Geophys. Res.*, *94*, 13,319–13,328.

Petersen, W. A., and S. A. Rutledge (1998), On the relationship between cloud-to-ground lightning and convective rainfall, *J. Geophys. Res.*, *103*, 14,025–14,040.

Pinto, I. R. C. A., O. Pinto Jr., R. M. L. Rocha, J. H. Diniz, A. M. Carvalho, and A. C. Filho (1999), Cloud-to-ground lightning in southeastern Brazil in 1993: 2. Time variations and flash characteristics, *J. Geophys. Res.*, *104*, 31,381–31,387.

Price, C., and M. Asfur (2002), An improved ELF/VLF method for globally geolocating sprite-producing lightning, *Geophys. Res. Lett.*, *29*(3), 1031, doi:10.1029/2001GL013519.

Reising, S. C., U. S. Inan, and T. F. Bell (1999), ELF sferic energy as a proxy indicator for sprite occurrence, *Geophys. Res. Lett.*, *26*, 987–990.

Rutledge, S. A., E. R. Williams, and T. D. Keenen (1992), The Down Under Doppler and Electricity Experiment (DUNDEE): Overview and preliminary results, *Bull. Am. Meteorol. Soc.*, *73*, 3–16.

Sato, M., and H. Fukunishi (2003), Global sprite occurrence locations and rates derived from triangulation of transient Schumann resonance events, *Geophys. Res. Lett.*, *30*(16), 1859, doi:10.1029/2003GL017291.

Shackford, C. R. (1960), Radar indications of a precipitation-lightning relationship in New England thunderstorms, *J. Meteorol.*, *17*, 15–19.

Tapia, A., J. A. Smith, and M. Dixon (1998), Estimation of convective rainfall from lightning observations, *J. Appl. Meteorol.*, *37*, 1497–1509.

Uman, M. A., Y. T. Lin, and E. P. Krider (1980), Errors in magnetic direction finding due to nonvertical lightning channels, *Radio Sci.*, *15*, 35–39.

Williams, E. R. (1985), Large-scale charge separation in thunderclouds, *J. Geophys. Res.*, *90*, 6013–6025.

Williams, E. R., S. A. Rutledge, S. G. Geotis, N. Renno, E. Rasmussen, and T. Rickenbach (1992), A radar and electrical study of tropical "hot towers", *J. Atmos. Sci.*, *49*(15), 1386–1395.

Williams, E. R., K. Rothkin, and D. Stevenson (2000), Global lightning variations caused by changes in thunderstorm flash rate and by changes in the number of thunderstorms, *J. Appl. Meteorol.*, *39*, 2223–2230.

Wood, T. G., and U. S. Inan (2002), Long-range tracking of thunderstorms using sferic measurements, *J. Geophys. Res.*, *107*(D21), 4553, doi:10.1029/2001JD002008.

Yamashita, M., and K. Sao (1974a), Some considerations of the polarization error in direction finding of atmospherics – I. Effect of the Earth's magnetic field, *J. Atmos. Terr. Phys.*, *36*, 1623–1632.

Yamashita, M., and K. Sao (1974b), Some considerations of the polarization error in direction finding of atmospherics – II. Effect of the inclined electric dipole, *J. Atmos. Terr. Phys.*, *36*, 1633–1641.

Zajac, B. A., and S. A. Rutledge (2001), Cloud-to-ground lightning activity in the contiguous United States from 1995 to 1999, *Mon. Weather Rev.*, *129*, 999–1019.

U. S. Inan and T. G. Wood, STAR Laboratory, Stanford University, Stanford, CA 94305-9515, USA. (twood@stanford.edu)